[Supporting Information] Exciton Dynamics from Strong to Weak Coupling Limit Illustrated on a Series of Squaraine Dimers

Merle I. S. Röhr,[†,‡] Henning Marciniak,[¶] Joscha Hoche,[†] Maximilian H. Schreck,[¶] Harald Ceymann,[¶] Roland Mitric,[*,†,‡] and Christoph Lambert[*,¶,‡]

†*Institut für Physikalische und Theoretische Chemie, Julius-Maximilians-Universität Würzburg, D-97074, Würzburg, Germany*
‡*Center for Nanosystems Chemistry, Julius-Maximilians-Universität Würzburg*
¶*Institut für Organische Chemie, Julius-Maximilians-Universität Würzburg, D-97074, Würzburg, Germany*

E-mail: roland.mitric@uni-wuerzburg.de; christoph.lambert@uni-wuerzburg.de

Exciton Theory

In the simplest excitonic system, a dimer, two excitonic states result as a consequence of the electronic coupling between the respective excited state of the monomers due to the dipole-dipole coupling J between them:[1,2]

$$J = \frac{1}{4\pi\epsilon_0 hc} \left(\frac{\vec{\mu}_A \vec{\mu}_B}{r_{AB}^3} - \frac{3\left(\vec{\mu}_A \vec{r}_{AB}\right)\left(\vec{\mu}_B \vec{r}_{AB}\right)}{r_{AB}^5} \right) \tag{1}$$

Here $\vec{\mu}_A$ and $\vec{\mu}_B$ are the transition dipole moments of monomer A and monomer B, $\vec{r}_{AB}$ is the center-to-center distance between them and ϵ_0, h, and c are the vacuum permittivity, the Planck constant and the vacuum speed of light, respectively. It can be seen from formula 1, that J depends critically on the relative orientation of the monomer transition dipole vectors and can even change sign.

The transition energies $E_\pm$ from the ground state to the so-called exciton states of the dimer can be calculated from J and from the monomer transition energies E_A and E_B as:[3–5]

$$E_\pm = \frac{1}{2}\left(E_A + E_B + W_A + W_B\right) \pm \frac{1}{2}\sqrt{\left(E_A - E_B + W_A - W_B\right)^2 + 4J^2} \tag{2}$$

where W_A and W_B are energy shifts of the monomer transition energies due to the dipole-dipole coupling. In the case of a homo dimer with $A = B$ the formula simplifies to:

$$E\pm = \left(E_A + W_A\right) \pm J \tag{3}$$

According to formulas 2 and 3 the coupling strength is tightly connected to the excitonic splitting, which can be obtained from spectroscopic data. It can be approximated as

$$J = \sqrt{\frac{\Delta E^2 - \left(E_A - E_B\right)^2}{4}}, \tag{4}$$

if the difference $W_A - W_B$ is neglected. Here ΔE is the difference between the energy of the

two excitonic states in the dimer.

The transition dipole moments $M_\pm$ from the ground state to the exciton states can be approximated from the monomer transition dipole moments as:[1,6,7]

$$\vec{M}_+ = \vec{M}_A \cos\theta + \vec{M}_B \sin\theta \tag{5}$$

and

$$\vec{M}_- = \vec{M}_A \sin\theta + \vec{M}_B \cos\theta \tag{6}$$

where θ is defined by $\tan 2\theta = \frac{J}{(E_A - E_B)}$. For two identical monomers, the formulas 5 and 6 simplify to:

$$\vec{M}_\pm = \frac{1}{\sqrt{2}} \left(\vec{M}_A \pm \vec{M}_B \right) \tag{7}$$

In this case, the transition dipole moments are oriented perpendicularly to each other and the transition strength is distributed between them depending on the angle between the monomer transition dipoles. In perfect parallel head-to-tail arrangement, the transition dipole moment $\vec{M}_-$ belongs to the upper exciton state (termed S_2 in the following) and vanishes, so the full transition strength is concentrated in the lower exciton state (S_1). This may be termed a J-dimer in analogy to J-aggregates.[8] In a parallel face-to-face arrangement on the other hand, it would be vice versa with the transition strength concentrated in the S_2-state.

Diabatization

For a system composed of 2 monomers with 2 adiabatic excited states $\{\psi_1, \psi_2\}$, which are formed due to the interaction of the localized electronic excited states of each monomer, we

can define the electronic Hamiltonian as:

$$\mathbf{H}_A = \begin{bmatrix} E_1^A & 0 \\ 0 & E_2^A \end{bmatrix} \tag{8}$$

with the excitation energies of the n-th state E_n^A. We can expand the adiabatic states into diabatic basis functions $\{\phi_1, \phi_2\}$ which are connected to the adiabatic ones by a unitary transformation matrix $\mathbf{C}$,

$$\phi_i = \sum_j C_{ij} \psi_j \tag{9}$$

with the matrix elements C_{ij}. The diabatic basis set ϕ_k is defined to be as close as possible to a state which is fully localized on the k-th monomer. To obtain the rotation matrix, following Troisi,[9] we make use of the relation between the transition dipole moments of the monomers and the dimer as,

$$\mathbf{C} = \arg \min_\Omega ||\vec{\mu}_A \Omega - \vec{\mu}_L|| \tag{10}$$

with the transition dipole moment between the electronic ground and the adiabatic excited states $\vec{\mu}_A$ and the transition dipole moment between the ground states and the localized adiabatic states $\vec{\mu}_L$. This is called the orthogonal Procrustes problem[10] with its general solution by a singular value decomposition of the matrix $\mathbf{M} = \vec{\mu}_A \cdot \vec{\mu}_L^{\mathbf{T}}$,[11]

$$\mathbf{M} = \mathbf{U}\mathbf{\Sigma}\mathbf{V}^{\mathbf{T}} \tag{11}$$

to write

$$\mathbf{C}^{\mathbf{T}} = \mathbf{U}\mathbf{V}^{\mathbf{T}}. \tag{12}$$

The matrix of the electronic Hamiltonian with the diabatic states can be calculated by the transformation matrix and the Hamiltonian of the adiabatic states. The diagonal elements represent the electronic site energies of the localized exciton states and the off-diagonal

element is the coupling between the two states

$$\mathbf{H}_D = \begin{bmatrix} H_{11} & V_{12} \\ V_{21} & H_{22} \end{bmatrix} = \mathbf{C} \begin{bmatrix} E_1^A & 0 \\ 0 & E_2^A \end{bmatrix} \mathbf{C^T}. \tag{13}$$

With the transformation matrix elements numbered in the following way:

$$C = \begin{bmatrix} C_{11} & C_{12} \\ C_{21} & C_{22} \end{bmatrix} \tag{14}$$

Thus we can define the degree of exciton localization as the difference between the absolute values of the first and second element in a row of the matrix $\mathbf{C}$ like $|C_{11}|-|C_{12}| = |C_{21}|-|C_{22}|$.

Synthetic Procedure

All synthetic preparations were performed in standard glassware. The chemicals used were purchased from commercial suppliers and utilised without further purification. Reactions under nitrogen atmosphere (dried over Sicapent form Merck; oxygen was removed by copper catalyst R3-11 from BASF) were carried out in oven-dried glass ware with solvents that were dried according to literature procedures and stored under nitrogen. Silica gel $32 - 64$ μm was used for flash chromatography.
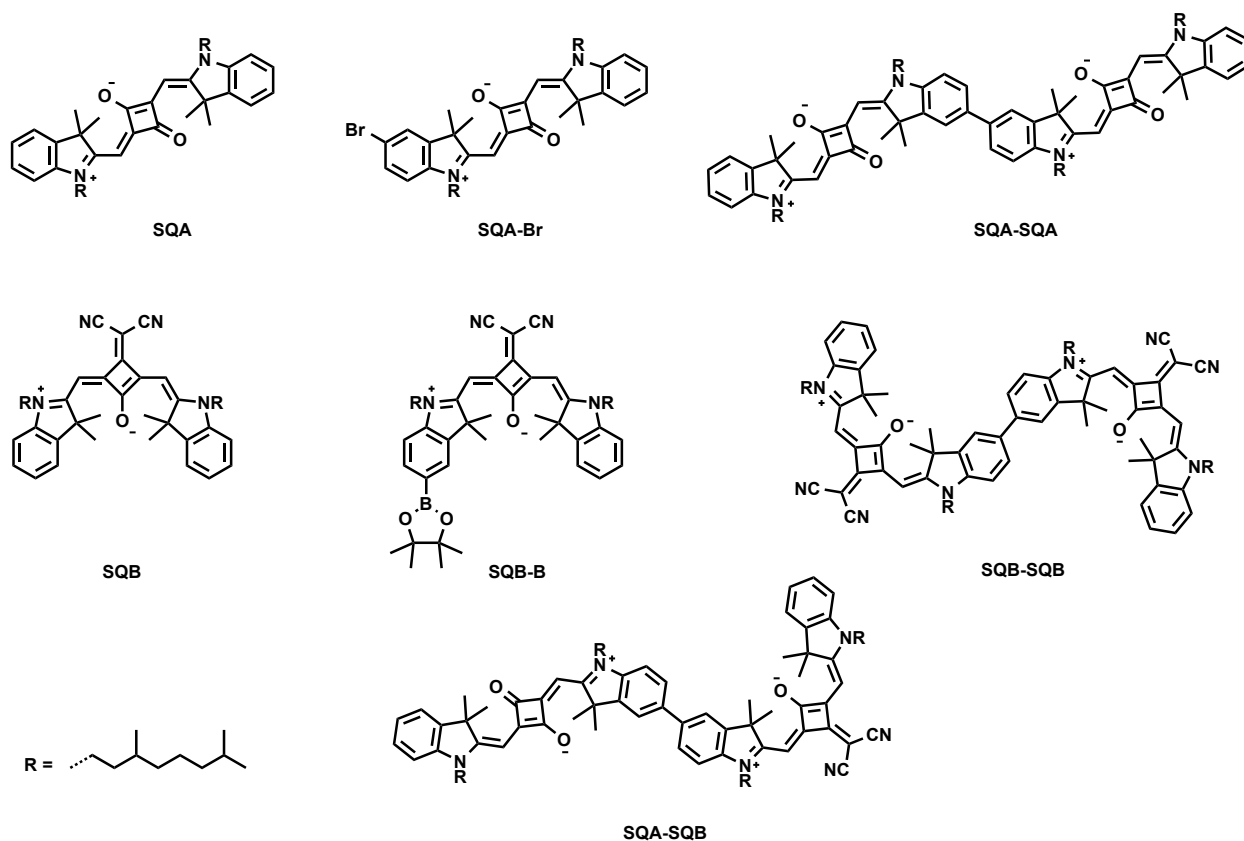
Scheme 1: Unfunctionalised monomeric model compounds **SQA** and **SQB**, precursors **SQA-Br**, **SQB-B**, homodimers **SQA-SQA** and **SQB-SQB**, and heterodimer **SQA-SQB**.

Compounds **SQA**,[12] **SQA-Br**,[13] **SQB**,[12] **SQB-B**,[14] **SQA-SQA**,[14] **SQB-SQB**[13] (cf. Scheme 1) were synthesized according to the given literature.
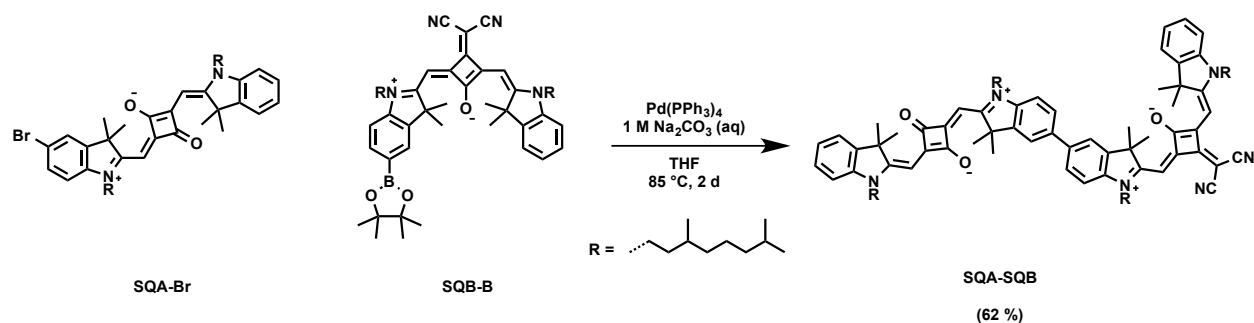
Scheme 2: Synthesis of the heterodimer **SQA-SQB**.

The squaraine heterodimer **SQA-SQB** was prepared via the Pd-catalysed *Suzuki* coupling reaction of **SQA-Br** and **SQB-B** using aqueous Na_2CO_3 as base in peroxide-free THF under continuous heating at 85 °C for 2 d (see Scheme 2).

NMR-Spectra were recorded on a Bruker Avance III HD 600 FT-spectrometer. The chemical shifts are given in ppm, relative to the internal standard tetramethylsilane (TMS). The coupling constants are indicated in Hertz (Hz). Abbreviations used for the spin multiplicities or for C-atom descriptions are: s = singlet, d = doublet, m = multiplet, dd = doublet of doublet; prim = primary, sec = secondary, tert = tertiary, quart = quaternary. Multiplet signals or overlapping signals in proton NMR spectra that could not be assigned to first order couplings are indicated as (-).

High resolution mass spectrometry was performed on a Bruker Daltonics microTOF focus (ESI) system.

Gel Permeation Chromatography (GPC) was carried out at 20 °C in chloroform with a Shimadzu instrument (incorporating a diode array detector (Model SPD-M20A), system controller (Model CBM-20A), solvent delivery unit (Model LC-20AD), and online degasser (Model DGU 20A9)). Preparative chromatography was performed in recycling mode on two consecutive SDV columns (PSS SDV preparative 50 Åand 500 Å, dimensions: 20 × 600 mm, particle size: 10 µm) from PSS/Mainz, Germany.

SQA-SQB
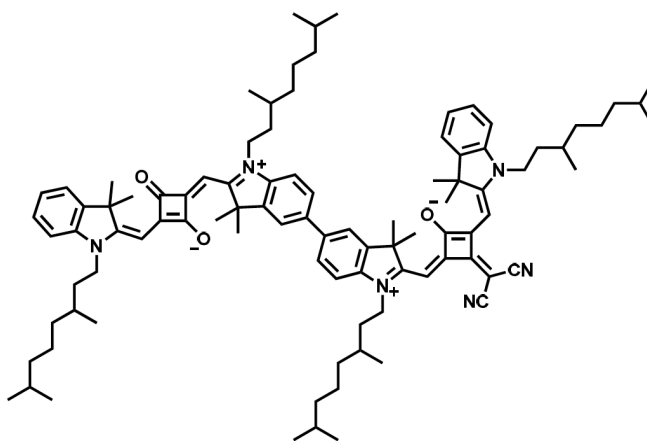
Scheme 3: Squaraine heterodimer **SQA-SQB**

Under a nitrogen atmosphere **SQA-Br** (70.0 mg, 92.6 µmol) and **SQB-B** (95.0 mg, 112 µmol) were dissolved in peroxide-free THF (7 ml). An aqueous solution of Na_2CO_3 (1 M, 278 µl, 278 µmol) was subsequently added and the mixture was purged in a gentle stream of nitrogen for 20 min. $Pd(PPh_3)_4$ (10.7 mg, 9.26 µmol) was added and the reaction was continuously heated at 85 °C for 2 d. The solvent was removed *in vacuo* and the residue purified by flash chromatography (eluent: DCM/MeOH = 99:1) and preparative recycling GPC ($CHCl_3$). Finally the product (cf. Scheme 3) was dissolved in a small amount of DCM and dripped into an excess of *n*-hexane. The mixture was allowed to stand overnight in the fridge at 4 °C. The precipitate formed was filtered off and dried under high vacuum.

Yield: 80.0 mg (57.1 µmol, 62%) of a bronze solid.

$C_{95}H_{126}N_6O_3$ [1400.06]

¹H-NMR (600.1 MHz, CD₂Cl₂):

δ [ppm] = 7.62-7.56 (-, 4H, CH), 7.42-7.31 (-, 4H, CH), 7.22 (dd, ^3J = 7.4 Hz, ^4J = 0.7 Hz, 1H, CH), 7.18-7.12 (-, 2H, CH), 7.08 (d, ^3J = 7.9 Hz, 1H, CH), 7.07 (d, ^3J = 8.2 Hz, 1H, CH), 7.02 (d, ^3J = 8.0 Hz, 1H, CH), 6.490 (s, 1H, CH), 6.487 (s, 1H, CH), 5.93-5.91 (-, 2H, CH), 4.14-3.95 (-, 8H, NCH₂), 1.88-1.72 (-, 28H, 4 × NCH₂CH, 8 × CH₃), 1.72-1.57 (-, 8H, 4 × NCH₂CH, 4 × CH), 1.57-1.48 (-, 4H, CH), 1.46-1.13 (-, 24H, CH₂), 1.08 (d, ^3J = 6.3 Hz, 3H, CH₃), 1.07 (d, ^3J = 6.4 Hz, 3H, CH3), 1.05 (d, ^3J = 6.4 Hz, 3H, CH₃), 1.03 (d, ^3J = 6.5Hz, 3H, CH₃), 0.89-0.84 (-, 24H, CH₃).
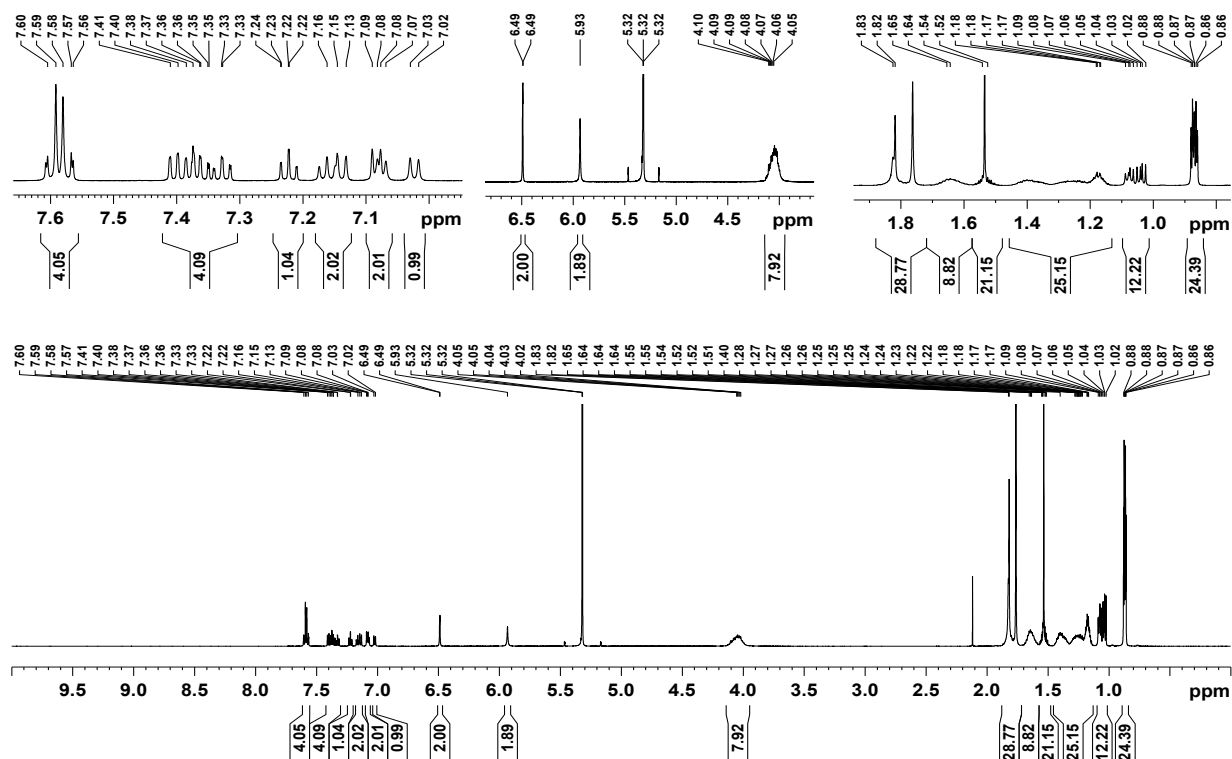
Fig. S1: ¹H-NMR spectrum of **SQA-SQB** recorded with 600.1 MHz NMR in CD₂Cl₂

¹³C-NMR (150.9 MHz, CD₂Cl₂):

δ [ppm] = 181.2 (2 × quart), 180.1 (quart), 179.4 (quart), 173.5 (quart), 172.3 (quart), 171.6 (quart), 170.3 (quart), 169.2 (quart), 167.9 (quart), 166.9 (quart), 166.3 (quart), 143.7 (quart),142.9 (2 × quart), 142.8 (quart), 142.7 (quart), 142.5 (quart), 142.3 (quart), 141.7 (quart), 137.8 (quart), 136.5 (quart), 128.4 (tert), 128.2 (tert), 127.1 (tert), 127.0 (tert), 124.9 (tert), 124.1 (tert), 122.63 (tert), 122.61 (tert), 121.2 (tert), 121.1 (tert), 119.18 (quart), 119.16 (quart), 110.8 (tert), 110.6 (tert), 109.9 (tert), 109.8 (tert), 89.6 (tert), 89.5 (tert), 87.1 (tert), 87.0 (tert), 49.89 (quart), 49.88 (quart), 49.7 (quart), 49.5 (quart), 43.4 (sec), 43.3 (sec), 42.5 (2 × sec), 40.6 (quart), 39.5 (4 × sec), 37.5 (2 × sec), 37.49 (sec), 37.47 (sec), 34.42 (sec), 34.39 (sec), 34.1 (2 × sec), 31.5 (2 × tert), 31.3 (2 × tert), 28.41 (tert), 28.40 (tert), 29.39 (tert), 28.38 (tert), 27.3 (2 × prim), 27.1 (2 × prim), 26.9 (prim), 26.8 (prim), 26.7 (prim), 26.6 (prim), 25.11 (sec), 25.09 (sec), 25.06 (sec), 25.03 (sec), 22.83 (2 × prim), 22.82 (2 × prim), 22.7 (4 × prim), 19.84 (prim), 19.81 (prim), 19.79 (prim), 19.77 (prim).
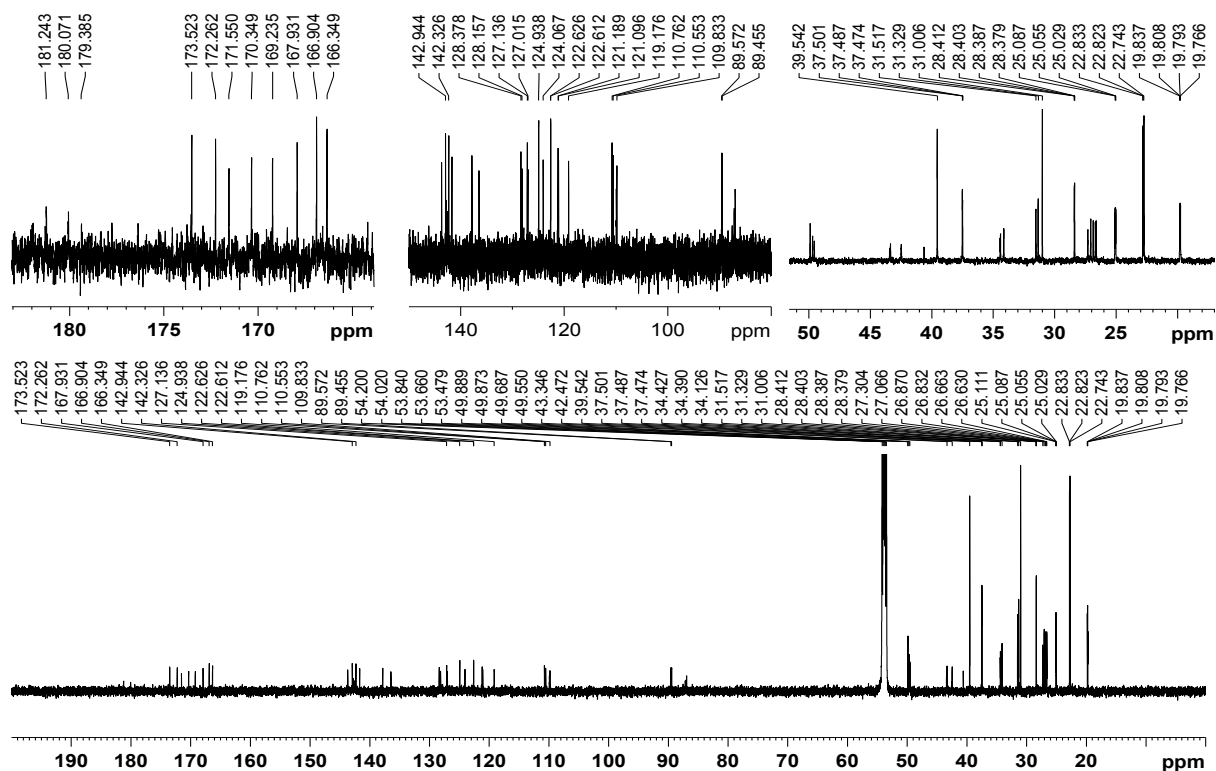
Fig. S2: ^{13}C NMR spectrum of **SQA-SQB** recorded with 150.9 MHz NMR in CD$_2$Cl$_2$

ESI-MS pos (high resolution): [M$^{\cdot+}$]

calc.:   1399.99186 m/z

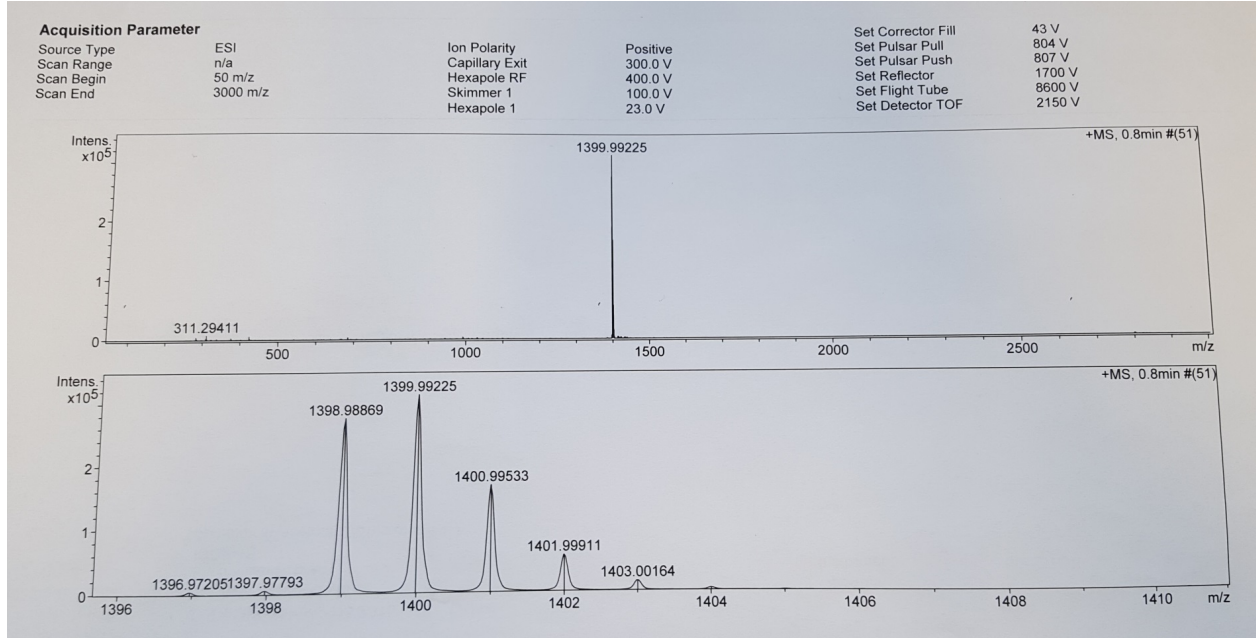found: 1399.99225 m/z $\Delta = 0.28$ ppm

Fig. S3: HRMS-ESI spectra (positive mode, acetonitrile/CHCl$_3$ 1:1) of **SQA-SQB**.

Field Induced Surface Hopping Simulations

In the FISH simulations, an ensemble of 200 classical trajectories is propagated in a manifold of several electronic states and the population transfer between these states is described by a stochastic hopping procedure, which is based on quantum state populations. Initial conditions for the trajectory simulations have been obtained by discrete sampling of a quantum mechanical Wigner distribution for the harmonic normal modes ω_n of the molecular system:[15,16]

$$\rho_{00}\left(\mathbf{q}_0, \mathbf{p}_0\right) = \prod_{n=1}^{N_{modes}} \frac{\alpha_n}{\pi\hbar} \exp\left[-\frac{\alpha_n}{\hbar\omega_n}\left(p_{0n}^2 + \omega^2 q_{0n}^2\right)\right] \tag{15}$$

where q_{0n} and p_{0n} denote the ground state normal coordinates and conjugate momenta, while $\alpha_n = \tanh\left(\hbar\omega_n/2k_bT\right)$ is a temperature dependent quantity. In the present simulations, T has been chosen to be 300 K, which corresponds to the conditions used in the experiment. For the nuclear dynamicsm the classical Newton equations were integrated using the velocity Verlet[17] algorithm with a time step of 0.1 fs. The electronic degrees of freedom were propa-

gated along the classical trajectories by solving the time-dependent Schrödinger equation in the manifold of the electronic ground and two excited states. The integration was performed employing the fourth order Runge Kutta procedure with a time step of 4 x 10^{-5} fs. In this manner, time-dependent electronic state populations are obtained, which are then used to calculate surface-hopping probabilities. The states are coupled by the laser field $\mathbf{E}$(t) via an electric dipole coupling operator

$$V_{ij} = -\mu_{ij} \left[\mathbf{R}(t) \right] \cdot \mathbf{E}(t) \tag{16}$$

as well as by the nonadiabatic coupling terms

$$D_{ij}(\mathbf{R}(t)) = \langle \Psi_i(\mathbf{R}(t)) | \frac{d\Psi_j(\mathbf{R}(t))}{dt} \rangle \tag{17}$$

$$i\hbar \dot{c}_i(t) = E_i(\mathbf{R}(t))c_i(t) - \sum_j \left[i\hbar D_{ij}(\mathbf{R}(t)) + \mu_{ij}(\mathbf{R}(t)) \cdot \mathbf{E}(t) \right] c_j(t), \tag{18}$$

Here, $c(t)$ are the expansion coefficients of the electronic wave function, expanded in the adiabatic basis, which can be used in order to calculate the density matrix elements as

$$\rho_{ij} = c_i^* c_j. \tag{19}$$

In order to decide, when a state switch occurs, we determine the hopping probability in each nuclear time step by evaluation of the change of the quantum-electronic-state populations ρ_{ii} as follows:

$$P_{i \to j} = \Theta(-\dot{\rho}_{ii})\Theta(\dot{\rho}_{jj})\frac{-\dot{\rho}_{ii}}{\rho_{ii}}\frac{\dot{\rho}_{jj}}{\sum_k \Theta(\dot{\rho}_{kk})\dot{\rho}_{kk}}\Delta t \tag{20}$$

Here the Θ-functions have a value of one for positive arguments and of zero otherwise. By averaging over an ensemble of independent trajectories, the real-time electronic-state population can be determined.

RICC2: Excitation levels to excited states

Table S1: Contributions of excitation levels to excited states wavefunctions of the SQA-SQA, SQB-SQB and SQA-SQB dimer at RICC2/def2-SVP level of theory.

system	state	E/cm^{-1}	% singles	% doubles
SQA-SQA	S_1	16615	86.75	13.25
	S_2	18148	86.41	13.59
SQB-SQB	S_1	15122	86.86	13.14
	S_2	16292	86.86	13.14
SQA-SQB	S_1	15486	86.87	13.13
	S_2	17744	87.04	12.96

Calculated vertical absorption spectra with and without side chains
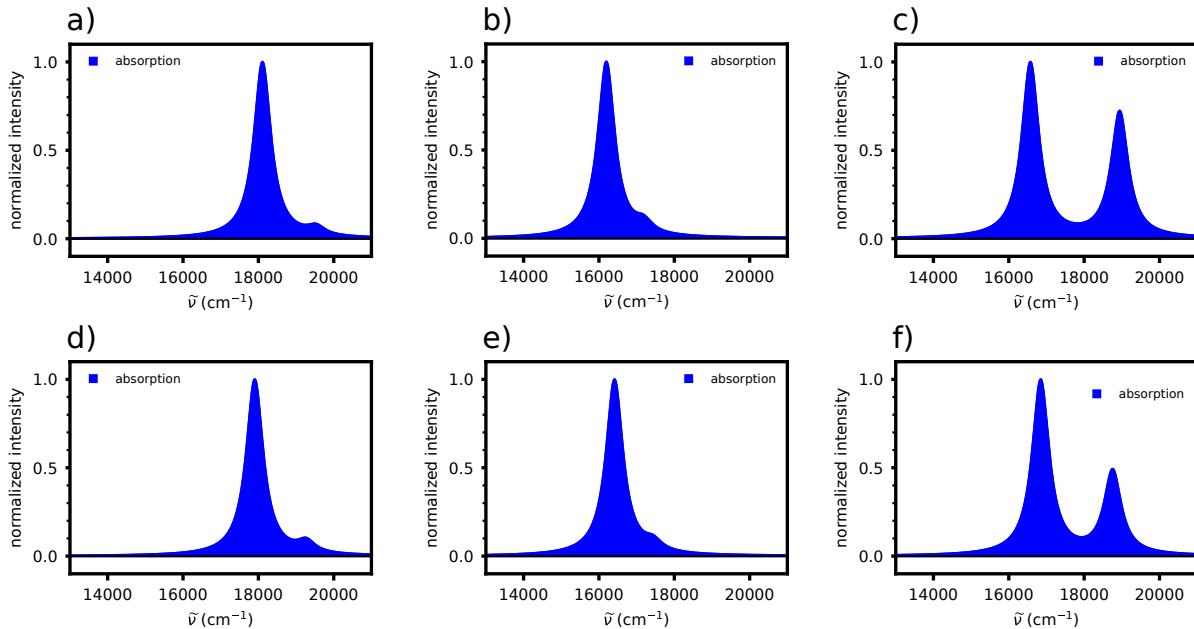
Fig. S4: Calculated vertical absorption spectra of **SQA-SQA** (a), **SQB-SQB** (b), and **SQA-SQB** dimer (c) in the ground state geometry without aliphatic chains. Calculated vertical absorption spectra of **SQA-SQA** (d), **SQB-SQB** (e), and **SQA-SQB** dimer (f) in the ground state geometry with aliphatic chains. The individual transitions have been convolved by a Lorentzian function with a width of 550 cm^{-1}.
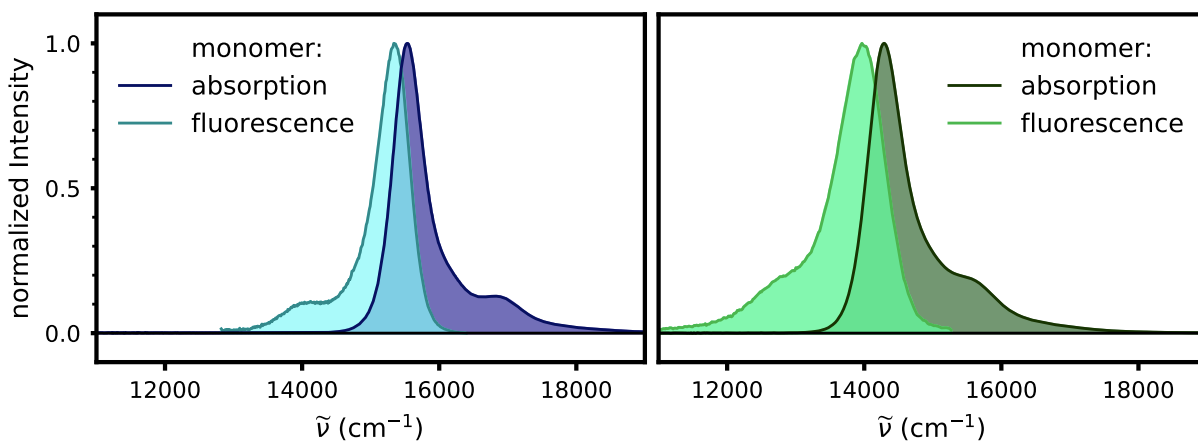
Absorption spectra of squaraine monomers

Fig. S5: (left) Experimental absorption and fluorescence spectrum (excitation at 16700 cm^{-1}) of **SQA** monomer in toluene. (right) Absorption and fluorescence spectrum (excitation at 15200 cm^{-1}) of **SQB** monomer.
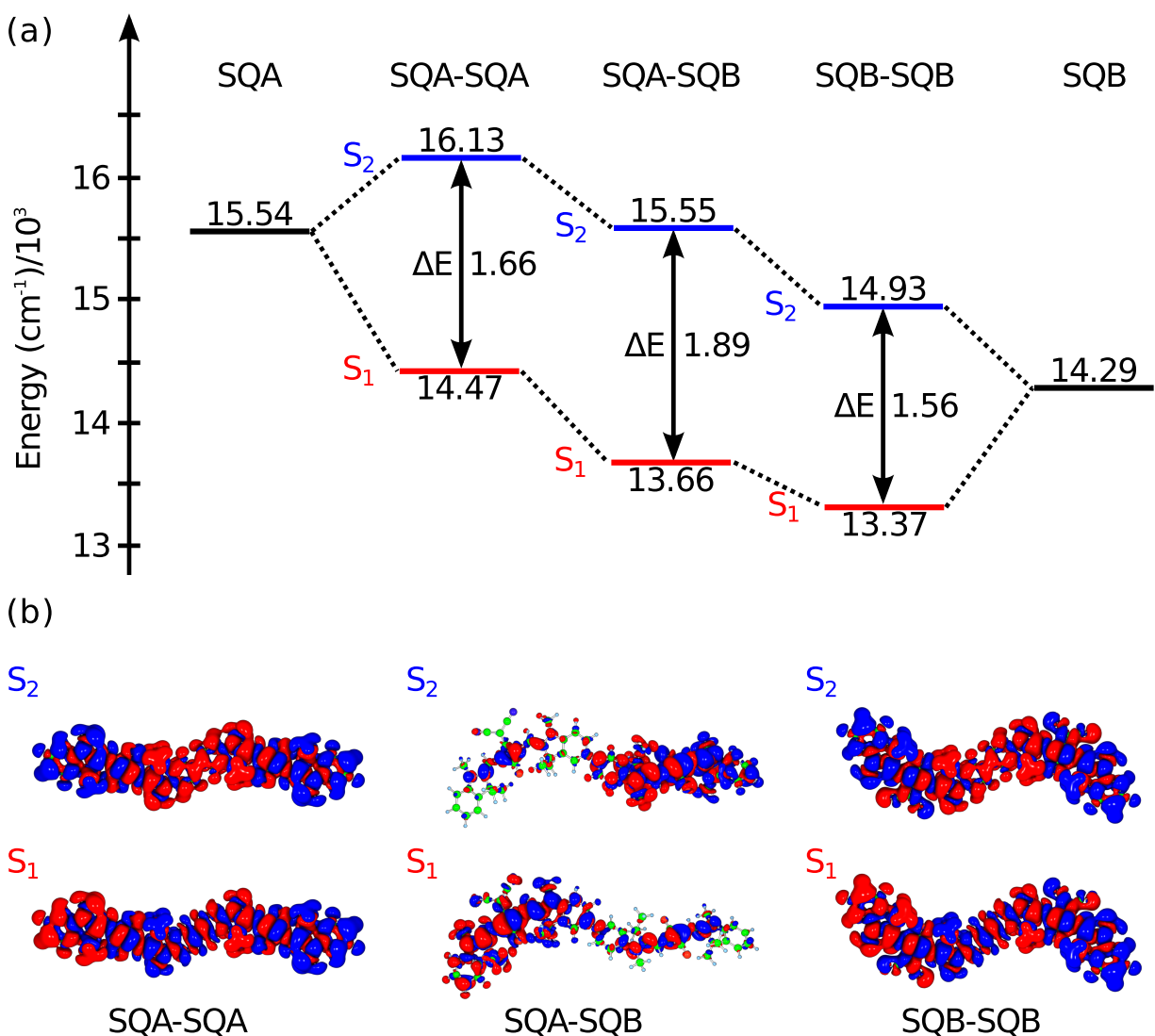
Analysis of the excited states

(a)

(b)

Fig. S6: (a) Diagram of the experimental absorption energies for the monomer and dimer systems. (b) The calculated transition densities are shown for the S_1 and S_2 electronically excited states of the dimer in the frame of CAM-B3LYP/def2-SVP and are done with the Multiwfn 3.4.1 software package.[18]
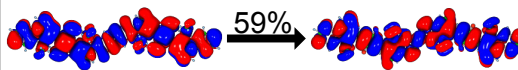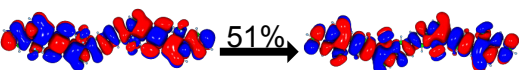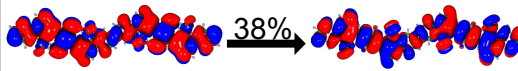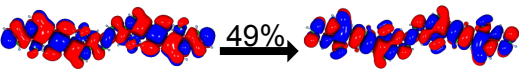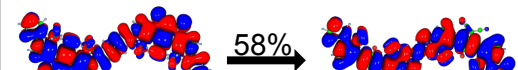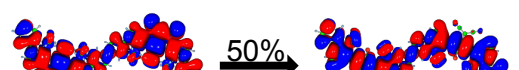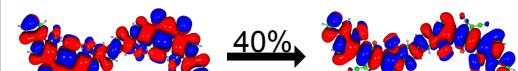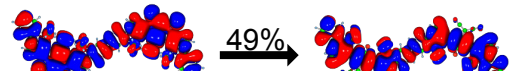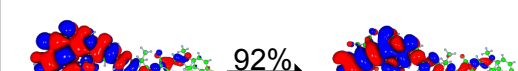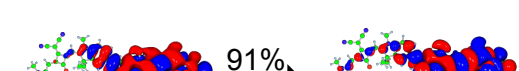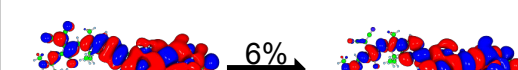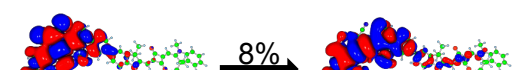
Fig. S7: Natural transition orbitals of the ground state geometry of all three dimer systems in the framework of TDDFT CAM-B3LYP/def-2SVP.

Transient absorption

The pump pulses for the transient absorption measurements were generated with a non-collinear optical parametric amplifier (NOPA) with two amplification stages, where wavelend harmonic of the Ti:sapphire laser source (Solstice, Newport Spectra-Physics) in nonlinear crystals (BBO).[19] The whitelight continuum seed is generated[20] by focusing pulses with a central wavelength of 1000 nm into a 3 mm thick sapphire plate. The 1000 nm pulses are generated by a TOPAS-C (Light Conversion), which is pumped by the Ti:sapphire fundamental beam (800 nm). The reason for employing 1000 nm pulses and not 800 nm pulses

directly from the Ti:sapphire laser is, to be able to also generate pump pulses with central wavelengths in the region around 800 nm, which would otherwise not be possible due to strong fluctuations of the resulting whitelight continuum in that region. The generated pump pulses were compressed with a fused silica prism compressor and attenuated with neutral density filters. They were focused into the sample and overlapped there with the probe pulses. The polarization relative to the probe pulses was set to magic angle (54.7^o) with two wire grid polarizers. As probe pulses, whitelight continuum pulses that were generated by focusing part of the 800 nm Ti:sapphire fundamental beam into a 3 mm thick sapphire plate, were employed. The pulses were focused into the sample to a spot size with 125 μm radius. Polarization was controlled with a wire grid polarizer. Time resolution was achieved by varying the path length of the 800 nm beam for probe pulse generation via a delay stage. The maximal time resolution can be estimated from the full width at half maximum of the cross correlation function of pump and probe pulses in the sample, which was 100 $\pm$ 20 fs, depending on pump and probe wavelength. The parameters of the pump pulses are given in Table S2.

Table S2: Pump parameters

	SQA-SQA		SQB-SQB		SQA-SQB	
central wavenumber [cm^{-1}]	14500	16100	13400	14900	13700	15600
pulse duration [fs]	20	23	21	21	21	24
pulse energy [nJ]	60	60	60	60	80	80
spot radius in sample [μm]	200	200	340	200	280	200
OD of sample at excitation wavenumber	0.32	0.11	0.45	0.18	0.32	0.22

Data processing

The transient absorption data was corrected for stray light from the excitation pulse by subtracting data from negative times, i.e. measurements where the probe pulse precedes the excitation pulse. For this purpose the data was converted from ΔOD to $10^{-\Delta OD}$ before subtraction and reconverted to ΔOD afterwards.

Furthermore, it was chirp corrected with a third order polynomial, that was fitted to time points of excitation and probe pulse overlap at 50 different wavelengths, which were identified by the signal rise.
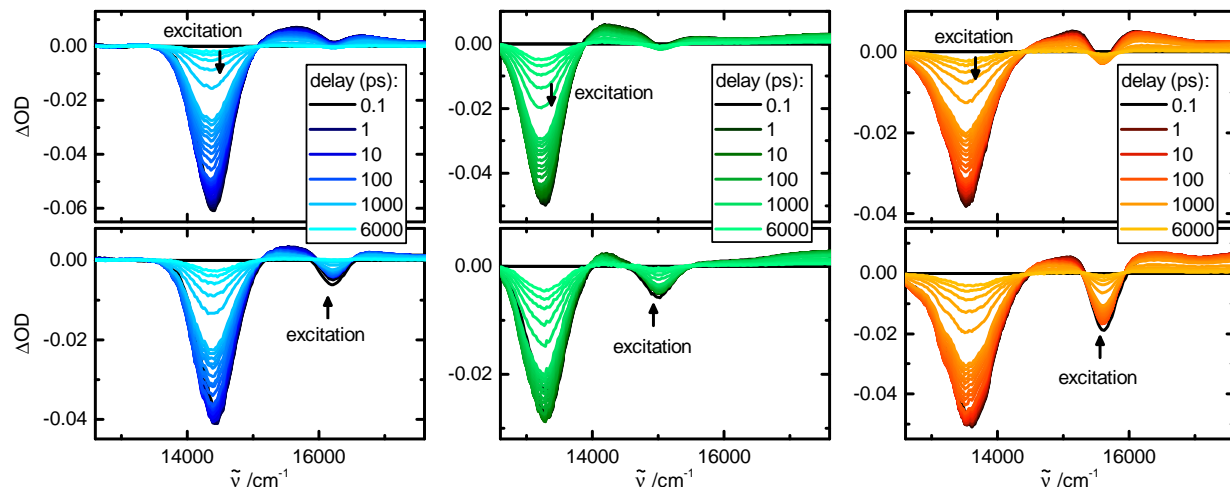

Fig. S8: Transient absorption spectra **SQA-SQA** (left), **SQB-SQB** (middle) and **SQA-SQB** (right) in toluene up to 6 ns after excitation at the indicated wavelengths.

Global fit information

The global fits were performed with a home-built LabView program, based on the Levenberg-Marquardt-algorithm. The cross correlation of pump and probe pulse is modeled by convolution of the exponential fit functions with a Gaussian function whose full width at half maximum (FWHM) is determined by the signal rise time. Coherent artifacts during the overlap of pump and probe pulse were accounted for by a gaussian function with the FWHM of the cross correlation function, and its first and second derivative.

Fluorescence lifetime fits

The FAST software (version 3.4.2) was used to fit the decay curves with an exponential decay function. Deconvolution of the data (4096 channels) was conducted by measuring

the instrument response function with a scatterer solution consisting of colloidal silicon in deionized water (LUDOX). The fluorescence quantum yields are given in Table S3.
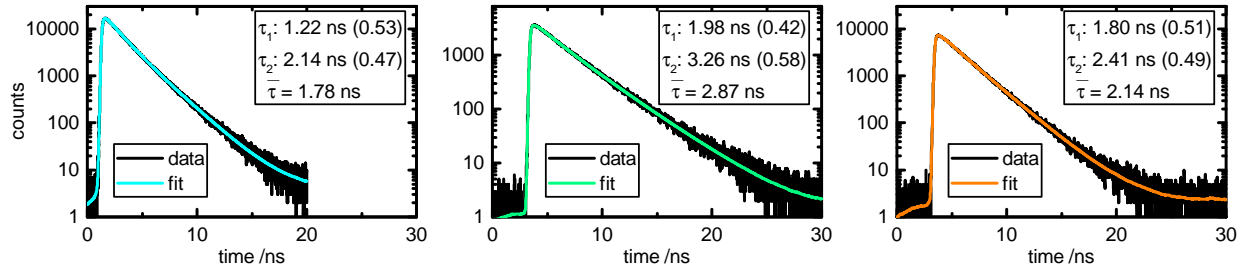

Fig. S9: Fits of TCSCP data of **SQA-SQA** (left), **SQB-SQB** (middle) and **SQA-SQB** (right) in toluene with exponential functions. The resulting time constants τ_i are given in the insets. The numbers in brackets give the relative contribution of the corresponding amplitudes to the decay. $\bar{\tau}$ is the expectation value of the lifetime.

Table S3: Fluorescence quantum yields Φ_{fl} of the SQA-SQA, SQB-SQB and SQA-SQB system.

	SQA-SQA^a	SQB-SQB^c	SQA-SQB^c
Φ_{fl}	0.82 ± 0.033	0.69 ± 0.020	0.69 ± 0.026

^{a} after excitation at 16700 cm^{-1}
^{b} after excitation at 15200 cm^{-1}
^{c} after excitation at 15600 cm^{-1}
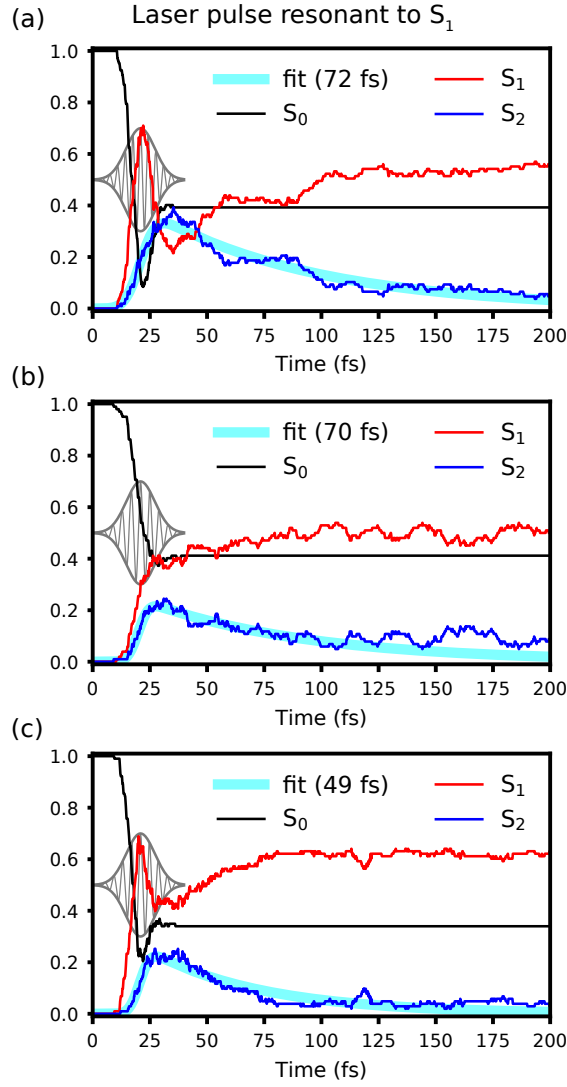
Dynamics in S_1

Fig. S10: Ensemble populations of the electronic states during the field-induced surface hopping dynamics of the **SQA-SQA** (a), **SQB-SQB** (b) and **SQA-SQB** (c) system with a laser pulse resonant to the S_1. The bold blue line shows the fit of the S_2 population to the following fit function: $F(t) = A \cdot \exp\left(-\frac{t-t_0}{\tau}\right) \cdot \exp\left(\frac{b^2}{4\sigma^2}\right) \cdot \left[1 + \mathrm{erf}\left(\frac{t-t_0-\frac{b^2}{2\sigma}}{b}\right)\right]$. Here, τ is the time constant for the population decay and t_0 is the center of the maximal field amplitude.

References

(1) Kasha, M.; Rawls, H.; Ashraf El-Bayoumi, M. The Exciton Model in Molecular Spectroscopy. *Pure Appl. Chem.* **1965**, *11*, 371–392.

(2) Seibt, J.; Marquetand, P.; Engel, V.; Chen, Z.; Dehm, V.; Würthner, F. On the Geometry Dependence of Molecular Dimer Spectra with an Application to Aggregates of Perylene Bisimide. *Chem. Phys.* **2006**, *328*, 354–362.

(3) Davydov, A. S. The Theory of Molecular Excitons. *Sov. Phys. Usp.* **1964**, *82*, 145–178.

(4) Schröter, M.; Pullerits, T.; Kühn, O. Unraveling the Quantum State Mixing of Excitonic and Vibronic Excitations in the Dynamics of Molecular Aggregates. *Ann. Phys.* **2015**, *527*, 536–545.

(5) Müller, A.; Talbot, F.; Leutwyler, S. S1/S2S1/S2 Exciton Splitting in the (2-pyridone)2(2-pyridone)2 Dimer. *J. Chem. Phys.* **2002**, *116*, 2836–2847.

(6) Ottiger, P.; Leutwyler, S. Excitonic Splitting and Coherent Electronic Energy Transfer in the Gas-Phase Benzoic Acid Dimer. *J. Chem. Phys.* **2012**, *137*, 204303.

(7) Ottiger, P.; Köppel, H.; Leutwyler, S. Excitonic Splittings in Molecular Dimers: Why Static Ab Initio Calculations Cannot Match them. *Chem. Sci.* **2015**, *6*, 6059–6068.

(8) Würthner, F.; Kaiser, T. E.; Saha-Möller, C. R. J-Aggregates: From Serendipitous Discovery to Supramolecular Engineering of Functional Dye Materials. *Angew. Chem. Int. Ed.* **2011**, *50*, 3376–3410.

(9) Arago, J.; Troisi, A. Dynamics of the Excitonic Coupling in Organic Crystals. *Phys. Rev. Lett.* **2015**, *114*, 026402.

(10) Berge, J. Procrustes Problems. *Psychometrika* **2005**, *70*, 799–801.

(11) Schönemann, P. H. A Generalized Solution of the Orthogonal Procrustes Problem. *Psychometrika* **1966**, *31*, 1–10.

(12) Völker, S. F.; Dellermann, T.; Ceymann, H.; Holzapfel, M.; Lambert, C. Synthesis, Electrochemical, and Optical Properties of Low Band Gap Homo- and Copolymers Based on Squaraine Dyes. *J. Polym. Sci. Pol. Chem* **2014**, *52*, 890–911.

(13) Ceymann, H.; Balkenhohl, M.; Schmiedel, A.; Holzapfel, M.; Lambert, C. Localised and Delocalised Excitons in Star-Like Squaraine Homo- and Heterotrimers. *Phys. Chem. Chem. Phys.* **2016**, *18*, 2646–2657.

(14) Ceymann, H.; Rosspeintner, A.; Schreck, M. H.; Mützel, C.; Stoy, A.; Vauthey, E.; Lambert, C. Cooperative Enhancement Versus Additivity of Two-Photon-Absorption Cross Sections in Linear and Branched Squaraine Superchromophores. *Phys. Chem. Chem. Phys* **2016**, *18*, 16404–16413.

(15) Wigner, E. On the Quantum Correction for Thermodynamic Equilibrium. *Phys. Rev.* **1932**, *40*, 749–759.

(16) Bonačić-Koutecký, V.; Mitrić, R. Theoretical Exploration of Ultrafast Dynamics in Atomic Clusters: Analysis and Control. *Chem. Rev.* **2005**, *105*, 11–65.

(17) Swope, W. C.; Andersen, H. C.; Berens, H. P.; Wilson, K. R. A Computer Simulation Method for the Calculation of Equilibrium Constants for the Formation of Physical Clusters of Molecules: Application to Small Water Clusters. *J. Chem. Phys.* **1982**, *76*, 637.

(18) Lu, T.; Chen, F. Multiwfn: A Multifunctional Wavefunction Analyzer. *J. Comput. Chem.* **2012**, *33*, 580–592.

(19) Riedle, E.; Beutter, M.; Lochbrunner, S.; Piel, J.; Schenkl, S.; Spörlein, S.; Zinth, W.

Generation of 10 to 50 fs Pulses Tunable through all of the Visible and the NIR. *Appl. Phys. B* **2000**, *71*, 457–465.

(20) Brodeaur, A.; Chin, S. Ultrafast White-Light Continuum Generation and Self-Focusing in Transparent Condensed Media. *JOSA B 16*, 637–650.